Spectrochimica Acta Part A: Molecular and Biomolecular Spectroscopy 225 (2020) 117478

Contents lists available at ScienceDirect

Spectrochimica Acta Part A: Molecular and Biomolecular Spectroscopy

journal homepage: www.elsevier.com/locate/saa

Absorption lines measurements of carbon disulfide at 4.6 μm with quantum cascade laser absorption spectroscopy

Chenguang Yang [a], Hao Deng [a,b], Yuanyuan Qian [a,b], Mingxing Li [a,b], Bing Chen [a], Zhenyu Xu [a], Ruifeng Kan [a,c,*]

[a] Key Laboratory of Environmental Optics and Technology, Anhui Institute of Optics and Fine Mechanics, Chinese Academy of Science, Hefei, Anhui 230031, China
[b] University of Science and Technology of China, Hefei, Anhui 230022, China
[c] Changchun Institute of Optics, Fine Mechanics and Physics, Chinese Academy of Sciences, Changchun 130033, China

ARTICLE INFO

Article history:
Received 14 July 2019
Received in revised form 18 August 2019
Accepted 18 August 2019
Available online 19 August 2019

Keywords:
Carbon disulfide
Quantum cascade laser
Mid-infrared spectroscopy
Spectroscopic parameters

ABSTRACT

We report measured line intensities and air- and self-broadening coefficients for fifty-one carbon disulfide transitions in the $\nu1 + \nu3$ band near 4.6 μm. This spectral region was chosen due to the strong carbon disulfide absorption strength and in the range of the mid-infrared atmospheric window for laser-based sensing applications. Spectroscopic parameters were determined by spectra measuring with quantum cascade laser direct absorption spectroscopy and multi-line fitting with Voigt lineshape. These measured results would facilitate the development of calibrated-free mid-infrared carbon disulfide sensors.

1. Introduction

Detection of carbon disulfide (CS_2) has significant importance in atmospheric environmental chemistry, medical diagnostics, etc. Although the concentration of CS_2 in atmosphere is lower than other common sulfides, it is the source of 30% carbonyl sulfide and would be oxidized into sulfide dioxide to form acid rain or haze [1]. It is also one of the typical odors, which would be absorbed by inhalation and skin and is toxic to the nerves, cardiovascular, reproductive, gastrointestinal, urinary and other systems [2]. The advisory permissible exposure limit value of CS_2 recommended by the National Institute of Occupational Safety and Health of the United States is 1 ppm [3], and the Chinese national one class standard value of CS_2 at boundary of industrial enterprises is 2 mg/m^3 [4]. In breath analysis area, CS_2 is a potential noninvasive marker of respiratory bacterial colonization in cystic fibrosis, and would be helpful to diagnose cirrhosis coronary, and artery diseases [5].

Unlike gas chromatography or diethylamine spectrophotometry, the traditional methods for CS_2 detection, optical spectroscopy has the advantage of fast response time and non-contact measurement. Using differential optical absorption spectroscopy, Yu et al. [6] and Zhang et al. [7] detected the CS_2 for air pollution control and online monitoring SF_6 decomposition, respectively. Du et al. [8,9] developed a sensitive CS_2 senor based on 4.6 μm mid-infrared wavelength modulation spectroscopy. Lendl et al. [10,11] also created a compact CS_2 sensor based on 4.6 μm quartz-enhanced photoacoustic spectroscopy.

According to the Pacific Northwest National Laboratory database [12], there are six main CS_2 absorption bands in mid-infrared range, $\nu3$-$\nu1$ band near 11.2 μm, $\nu3$ band near 6.7 μm, $\nu1 + \nu3$ band near 4.6 μm, $2\nu2 + \nu3$ band near 4.3 μm, $2\nu1 + \nu3$ band near 3.5 μm and $\nu1 + 2\nu2 + \nu3$ band near 3.36 μm. The $\nu3$ band near 6.7 μm is the strongest of them, but would be interfered by water vapor seriously. The $\nu1 + \nu3$ band near 4.6 μm, the second strongest band, is within the range of the mid-infrared atmospheric window. The recent availability of compact quantum cascade laser in the mid-infrared has led to the development of highly sensitive and low-interference diagnostics for carbon disulfide utilizing CS_2 transitions of $\nu1 + \nu3$ band as mentioned before [8–11]. For laser absorption measurements to be accurate and calibration-free, a comprehensive characterization of the fundamental spectroscopy is required in the wavelength domain of interest.

Although HITRAN database has not contained the lines parameters of CS_2, several studies on CS_2 spectroscopy by Blanquet et al. [13–17] have been reported in the literatures during the past two decades. They measured the line intensities of CS_2 $\nu3$ band [13], and the collision broadening coefficients of $\nu3$ and $\nu1 + \nu3$ bands caused by kinds of components, including N_2, O_2 and rare gases [14–16], with TDL spectroscopic technique. They also measured the line positions of CS_2 $2\nu1 + \nu3$ and $\nu1 + 2\nu2 + \nu3$ bands with FTIR spectroscopic technique. [17] However, the spectral parameters measurement for the $\nu1 + \nu3$ band near 4.6 μm, which has applied for CS_2 detection, is still rare. This motivates the current high-resolution spectroscopic study of the $\nu1 + \nu3$ band of CS_2.

* Corresponding author at: Key Laboratory of Environmental Optics and Technology, Anhui Institute of Optics and Fine Mechanics, Chinese Academy of Science, Hefei, Anhui 230031, China.
E-mail address: rfkan@ciomp.ac.cn (R. Kan).

https://doi.org/10.1016/j.saa.2019.117478
1386-1425/

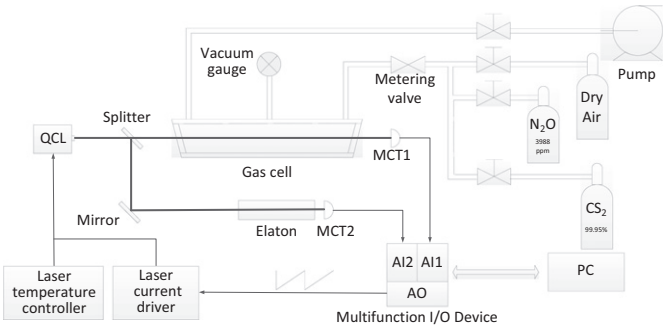

Fig. 1. Diagram of the experiment setup for the spectroscopic parameter measurements. QCL-quantum cascade laser, AO-Analog Output, AI-Analog Input, MCT-mercury cadmium telluride infrared detector, PC-Personal Computer.

In this paper, the spectral parameters of several dozen CS_2 absorption lines near 4.6 μm, including wavenumbers, line strengths, self- and air-broadening coefficients, are measured with quantum cascade laser absorption spectroscopy for our development of calibrated-free CS_2 sensing system. To our best knowledge this is the first relatively comprehensive experimental study of CS_2 spectral parameters near 4.6 μm for atmosphere detection.

2. Experimental setup

The diagram of the experimental setup is shown in Fig. 1. The emission wavenumber of the QCL laser used in this experiment (HAMAMATSU, LE0809QCL) can be turned from 2179 cm^{-1} to 2182 cm^{-1} by changing both operating temperature and forward current with the commercial temperature controller (Wavelength Electronics, TC15

Table 1
Spectroscopic parameters of CS_2 transitions measured in this work.

No	Position (cm^{-1})	Err (cm^{-1})	S @ 25 °C (cm^{-1}/(molec * cm^{-2}))	Err (%)	γ_{self} @ 25 °C (cm^{-1}/atm)	Err (%)	γ_{air} @ 25 °C (cm^{-1}/atm)	Err (%)
1	2179.1576	8E-4	4.2485E-22	0.88	0.1045	2.40	–	–
2	2179.2124	8E-4	1.1235E-21	0.26	0.0885	0.92	0.0915	1.10
3	2179.2644	8E-4	8.7596E-21	0.27	0.0907	1.52	0.0979	1.12
4	2179.3067	8E-4	4.2485E-22	0.88	0.1022	3.33	0.1192	4.06
5	2179.3322	7E-4	1.0869E-21	0.48	0.0877	1.48	0.0946	1.69
6	2179.4019	7E-4	6.6683E-22	0.60	0.0987	1.34	0.1122	3.45
7	2179.4539	6E-4	3.9821E-22	0.47	0.0895	1.21	0.1024	3.33
8	2179.4989	5E-4	1.0408E-21	0.40	0.0851	1.65	0.0948	2.75
9	2179.5992	5E-4	4.5390E-22	1.28	0.0991	1.24	–	–
10	2179.6132	4E-4	1.0215E-21	0.39	0.0801	1.31	0.1054	3.64
11	2179.7432	2E-4	4.1005E-22	0.94	–	–	–	–
12	2179.7558	2E-4	7.8467E-22	1.98	–	–	0.1031	1.83
13	2179.7784	2E-4	9.4566E-21	0.47	0.0900	4.26	0.0974	1.37
14	2179.8873	1E-4	1.4009E-21	0.49	0.0803	1.47	0.0905	1.55
15	2180.0266	1E-4	4.1096E-22	0.72	0.0965	3.28	0.1152	4.96
16	2180.0525	1E-4	9.4380E-22	0.35	0.0825	1.23	0.0941	3.20
17	2180.1038	1E-4	7.3232E-22	0.66	0.0964	2.92	0.0905	1.89
18	2180.1572	4E-4	8.6628E-22	1.12	0.0787	4.80	0.0860	1.79
19	2180.1662	5E-4	3.8152E-22	1.38	0.0841	5.11	0.0863	4.45
20	2180.2869	5E-4	7.9765E-21	1.09	0.0877	4.90	0.0952	1.63
21	2180.3034	4E-4	4.0744E-22	3.89	–	–	0.0925	4.79
22	2180.3200	4E-4	8.7391E-22	1.21	–	–	0.0825	2.69
23	2180.4184	4E-4	8.8042E-22	0.68	0.0845	3.00	0.0878	2.16
24	2180.4389	4E-4	4.0050E-22	1.75	0.0971	6.44	0.0845	5.57
25	2180.4450	4E-4	7.0344E-22	1.50	0.0902	4.98	0.1007	2.76
26	2180.5727	4E-4	3.8301E-22	2.24	–	–	0.0848	3.74
27	2180.5799	4E-4	8.2976E-22	1.21	0.0715	3.21	0.0821	5.35
28	2180.6731	6E-4	7.3614E-22	0.92	0.0745	4.87	0.0813	4.60
29	2180.7049	6E-4	3.1124E-22	1.34	0.0738	4.41	0.0919	5.08
30	2180.7788	5E-4	7.0863E-22	1.63	–	–	0.0758	2.86
31	2180.7873	5E-4	7.5782E-21	0.75	0.0928	2.49	0.0953	1.42
32	2180.8339	5E-4	1.1176E-21	0.63	0.0784	2.19	0.0846	3.10
33	2180.9209	7E-4	7.5277E-22	0.32	0.0776	1.43	0.0899	4.07
34	2180.9640	7E-4	3.7731E-22	1.03	0.0934	3.02	0.0980	5.25
35	2181.0147	5E-4	3.7731E-22	1.03	–	–	–	–
36	2181.0802	5E-4	7.2750E-22	0.43	0.0821	2.46	0.0812	3.62
37	2181.0911	5E-4	3.4006E-22	0.86	0.0855	1.95	0.0786	2.08
38	2181.1055	6E-4	7.4843E-22	0.51	0.0888	2.10	0.0782	2.73
39	2181.1621	5E-4	6.7459E-22	0.41	0.0773	1.58	0.0966	3.97
40	2181.2165	5E-4	3.2561E-22	1.24	0.0913	2.91	0.0787	3.22
41	2181.2805	5E-4	7.1782E-21	0.41	0.0918	1.95	0.0937	1.81
42	2181.3203	5E-4	6.3148E-22	0.53	0.0781	2.56	0.0863	4.02
43	2181.3402	6E-4	3.0495E-22	0.96	0.0805	2.78	0.0821	5.37
44	2181.3966	5E-4	6.7870E-22	0.45	0.0800	0.87	0.0909	2.42
45	2181.4255	5E-4	7.4804E-22	0.53	0.0854	1.68	0.0898	2.99
46	2181.4621	5E-4	3.1649E-22	1.06	0.0853	3.01	–	–
47	2181.5537	5E-4	5.9689E-22	0.54	0.0791	1.60	0.0756	3.07
48	2181.5824	6E-4	3.1099E-22	1.12	0.0597	5.75	–	–
49	2181.6243	5E-4	5.9881E-22	1.21	0.0837	4.50	–	–
50	2181.7011	6E-4	3.4717E-22	3.92		–	–	–
51	2181.7388	4E-4	7.5864E-22	4.22		–	–	–

Note: The Error of Position corresponds to one standard deviation (1 σ) of line positions measured with pure standard CS_2 gas in different pressure. The Errors of S @ 25 °C, γ_{self} @ 25 °C and γ_{air} @ 25 °C correspond to relative one standard deviation (1 σ) obtained from the linear fit.

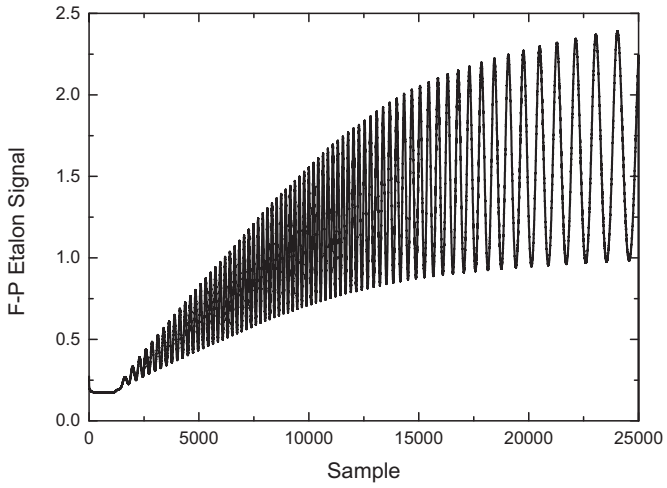

Fig. 2. The Fabry–Pérot (F-P) etalon signal with the wavelength turning of the QCL laser at 40 °C operation temperature.

LAB) and current driver (Wavelength Electronics, QCL1500 LAB). The laser beam is divided by the splitter into two paths, the measurement path and the reference path. The measurement path is addressed to the 10 cm gas cell and the transmitted laser beam is detected by a MCT detector (Vigo, PVI-4TE-10.6-20M). The reference path passes through the homemade germanium Fabry–Pérot (F-P) etalon, the designed free spectral range (FSR) of which is 0.025 cm^{-1}, and detected by another MCT detector with the same model. The detected signals are acquired by the multifunction I/O device (NI Corporation, USB-6361) with 250 kS/s sample rate for post-processing analysis.

The stated concentration nitrous oxide (3988 ppm) is used for laser absolute wavenumber calibration. In the lines' positions, intensities and self-broadening coefficients experiments, the spectrums of the commercial pure CS_2 gas sample (better than 99.95%) under different pressures are attained. And in the lines' air-broadening coefficients experiments, the spectrums of manually mix gas, which contains about 1% pure CS_2 and 99% pure dry air, are measured under several pressures. The pressure in the gas cell is monitoring by a high precision vacuum gauge (Pfeiffer, CMR361) with 0.2% uncertainty. The limited vacuum and vacuum leak rate of the gas cell are 15 Pa and 10^{-9} Pa $*$ m^3/s. All measurements are done at room temperature (approximately 25 ± 1 °C).

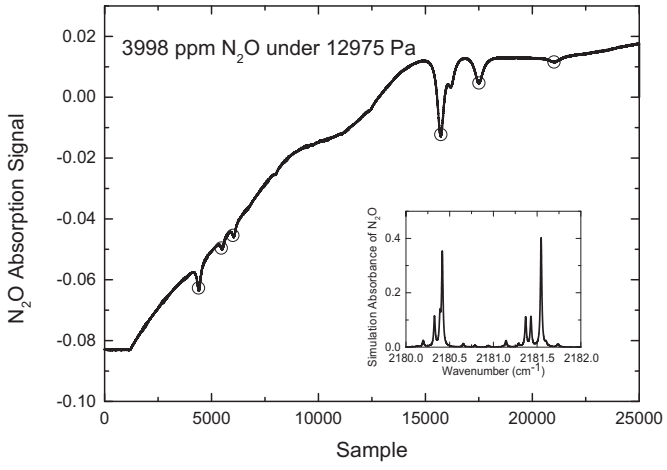

Fig. 3. The nitrous oxide absorption signal and the absorption simulation under the same condition.

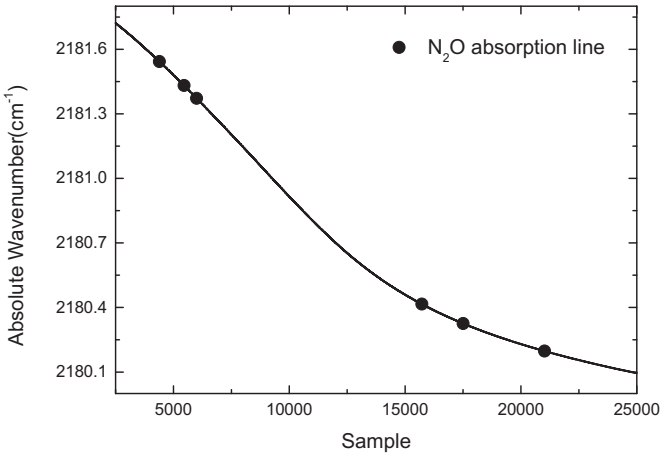

Fig. 4. The absolute wavenumber tuning of the laser and the six calibration nitrous oxide absorption line position.

3. Data retrieval method

The method used for TDLAS signal processing has been described in detail in [18]. Hereafter, we recapitulate the main points. According to the Beer-Lambert Law, the transmitted laser intensity $I(\nu)$ can be expressed as

$$I(\nu) = I_0(\nu)\ \exp(-\alpha(\nu)L) = I_0(\nu)\ \exp(-SN\varphi(\nu)L). \quad (1)$$

Here $I_0(\nu)$ is the incident laser intensity at wavenumber ν, and absorption coefficient $\alpha(\nu)$ can be expressed as the product of the line strength S, the number density N and the line-shape function $\varphi(\nu)$. L is the length of the medium.

Based on the ideal gas equation, the number density N at certain pressure P and temperature T can be calculated by

$$N = \frac{P\,T_0}{P_0\,T} N_0. \quad (2)$$

Here N_0 (2.6875×10^{19} molec/cm^3) is the number density of ideal gas at standard pressure P_0 (1 atm) and temperature T_0 (273.15 K). The line-shape function is a normalized function. Therefore, the integrated absorbance area A can be described as

$$A = \int_{-\infty}^{+\infty} SN\varphi(\nu)Ld\nu = SNL\int_{-\infty}^{+\infty} \varphi(\nu)d\nu = SNL. \quad (3)$$

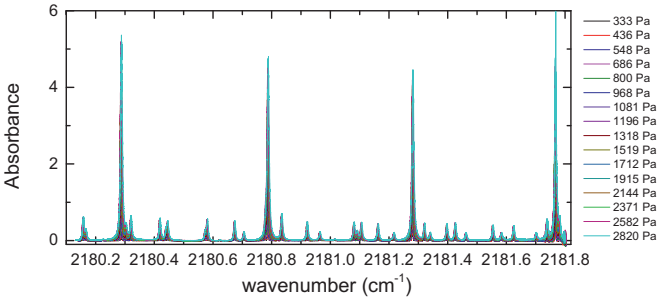

Fig. 5. Absorbance of 99.95% CS_2 in 10 cm gas cell at 25 °C and different pressure.

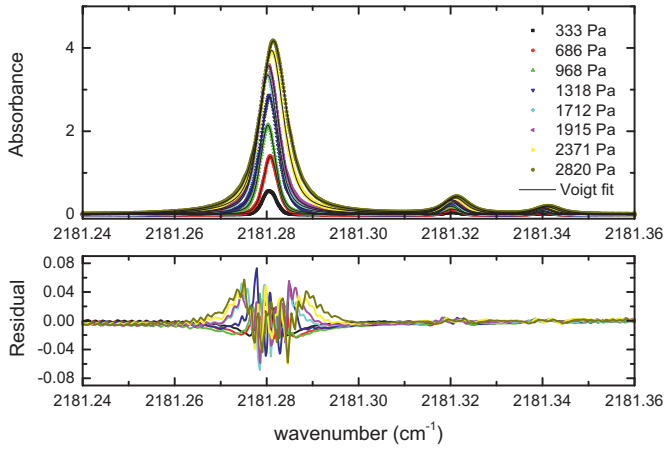

Fig. 6. An example of the recorded absorption spectrum (dots) and the Voigt fitting (line) for the CS_2 spectra lines under different pressures (upper panel). Lower panel shows the observed minus calculated residual.

On the other hand, considering the effects of both Doppler and collision broadening, the line-shape function is standard Voigt model,

$$\varphi_V(\xi,\mu) = C\left(\frac{\mu}{\pi}\int_{-\infty}^{+\infty}\frac{e^{-t^2}}{(\xi-t)^2+\mu^2}dt\right) \tag{4}$$

where $C = \sqrt{\frac{\ln 2}{\pi}}\frac{1}{\Delta\nu_D}, \xi = \sqrt{\ln 2}\frac{\Delta\nu_L}{\Delta\nu_D}, \mu = \sqrt{\ln 2}\frac{\nu-\nu_0}{\Delta\nu_D}$.

Here, ν_0 is the center number of the transition, $\Delta\nu_D$ and $\Delta\nu_L$ are the half-width at half maximum (HWHM) of the Doppler and collision broadening respectively.

$\Delta\nu_D$ is the function of temperature T, molecular weight M and center number of the transition ν_0,

$$\Delta\nu_D = 3.58\times10^{-7}\nu_0\sqrt{\frac{T}{M}}. \tag{5}$$

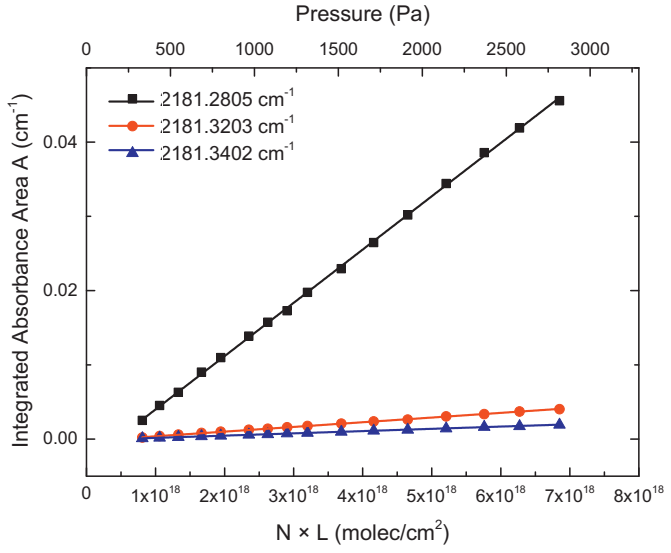

Fig. 7. Example of calculation of line intensity for CS_2 spectra lines.

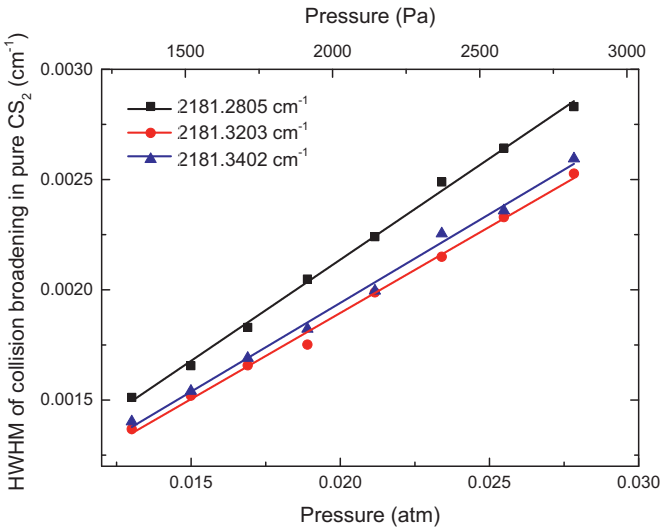

Fig. 8. Example of calculation of self-broadening coefficient for CS_2 spectra lines.

And, in the air, $\Delta\nu_L$ is the sum of air collision broadening and self-collision broadening, which can be written as

$$\Delta\nu_L = \gamma_{air}(P_{total}-P_{self})\left(\frac{T_0}{T}\right)^{n_{air}} + \gamma_{self}P_{self}\left(\frac{T_0}{T}\right)^{n_{self}} \tag{6}$$

with the sample total pressure P_{total} and the absorbing species partial pressure P_{self} at the temperature T. γ_{air} and γ_{self} are named as air-broadening coefficient and self-broadening coefficient respectively. n_{air} is the coefficient of temperature dependence of air-broadened half-width, and n_{self}, the coefficient of temperature dependence of self-broadened half-width, equals to 0.5 for hard sphere assumption.

The absolute wavenumber of the laser is determined by the etalon and the known nitrous oxide spectral line positions in the HITRAN [19] to measure the line positions of CS_2. A homemade fitting program based on Levenberg-Marquardt nonlinear least-squares fitting algorithm [18] is used to derive the integrated absorbance area A and the collision broadening $\Delta\nu_L$. By measuring and fitting the absorption lines of pure standard CS_2 gas in different pressure, line intensity S and self-broadening coefficient γ_{self} would be linearly regressed based on Eqs. (3) and (6). Then the absorption lines of 1% dry air mixed CS_2 gases with different pressures are measured and fitted to calculate air-

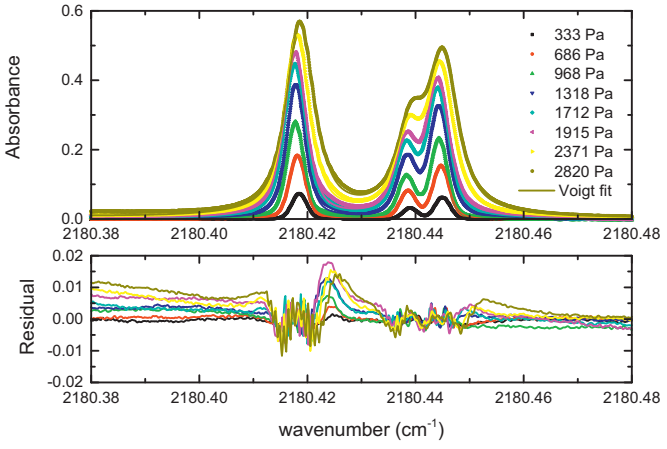

Fig. 9. Another example of the recorded absorption spectrum (dots) and the Voigt fitting (line) for the relatively weak spectra lines of CS_2 under different pressures (upper panel). Lower panel shows the observed minus calculated residual

broadening coefficient γ_{air} based on Eq. (6), ignoring the deviation caused by self-collision broadening..

4. Results and discussion

The line positions, intensities, self- and air-broadening coefficients of CS_2 fifty-one spectral transitions were studied between 2179 and 2182 cm^{-1}. Theses transitions are listed in Table 1. For line intensity calculation, the spectrums under sixteen pressures from 300 to 3000 Pa are measured. Eight of them with high pressures are used to calculate self-broadening coefficients. To determine the air-broadening coefficients of these lines, another eight spectrums are measured under the pressures from 900 to 8000 Pa. To the best of our knowledge, the present study is the first to provide parameters for these CS_2 lines.

4.1. Laser absolute wavenumber calibration

The relative wavenumber of the QCL laser is easily derived from the peak and valley positions of the F-P etalon signal, as shown in Fig. 2. However, besides the lack of absolute wavenumber calibration, the actual FSR of the etalon also has deviation from designed value, 0.025 cm^{-1}, because of the divergence between the etalon's optical axis and the incident beam.

Therefore, by measurement 3998 ppm nitrous oxide absorption spectrum under 12,975 Pa, six nitrous oxide absorption lines in this range, which is marked with "O" in Fig. 3, are used for calibrate the absolute wavenumber and the actual FSR in the measurement. The absolute wavenumber of laser at the sample of the fourth absorption line is calibrated to be 2180.41585 cm^{-1}, which is simulated with HITRAN12 [20] as shown in the inset of Fig. 3. The actual FSR is calibrated to be 0.0242 cm^{-1} by minimizing the residuals of the other five line positions, all of which are less than 0.001 cm^{-1}.

The absolute wavenumber of the laser at 40 °C operation temperature is shown in Fig. 4 by spline interpolating the calibrated F-P etalon result. The processes of the laser absolute wavenumber calibration for other operation temperatures are similar.

4.2. Line positions, intensities, and self-broadening coefficients measurement

The absorption-free baseline is piecewise fitted with the lowest pressure absorption spectrum, and subtracted to obtain the absorbance spectrum under sixteen different pressures. As shown in Fig. 5, there are four main absorptions in the laser wavenumber tuning range, the absorbance of them decrease with the increase of wavenumber. As the signal-to-noise ratio increases with the laser's power, the noise of the absorbance is much larger near 2181.8 cm^{-1}, the beginning of the laser tuning range, which causes the impression of absorbance.

All of the absorbance spectrums in Fig. 5 are divided into thirteen pieces and fitted with Voigt profit under the fixed Doppler broadening, which is calculated by Eq. (5) assuming the temperature of sample gas maintain 25 °C, to obtain the line position, integrated absorbance area and HWHM of collision broadening. Fig. 6 presents representative measured and fitted absorption spectrums near 2181.3 cm^{-1} and the residuals between them in eight typical pressures. The positions of three absorption lines are determined by averaging those sixteen times fitting results, equal to 2181.2805 cm^{-1}, 2181.3203 cm^{-1} and 2181.3402 cm^{-1}. As shown in Fig. 7, the linear correlation coefficients between the integrated absorbance areas and the products of the molecular density and the optical path length are all better than 0.999, and the line intensities are obtained by regression statistics to be 7.1782×10^{-21} $cm^{-1}/(molec * cm^{-2})$ for line at 2181.2805 cm^{-1}, and 6.3148×10^{-22} $cm^{-1}/(molec * cm^{-2})$ for line at 2181.3203 cm^{-1} and 3.0495×10^{-22} $cm^{-1}/(molec * cm^{-2})$ for line at 2181.3402 cm^{-1}. Similarly, the linear correlation coefficients between the gas pressure, from 1318 Pa to 2820 Pa, and the HWHM of collision broadening are also better than 0.99 as demonstrated in Fig. 8. The self-broadening coefficients are 0.0918 cm^{-1}/atm for line at 2181.2805 cm^{-1}, 0.0781 cm^{-1}/atm for line at 2181.3203 cm^{-1} and 0.0805 cm^{-1}/atm for line at 2181.3402 cm^{-1}. Another example of representative measured and fitted absorption spectrums is shown in Fig. 9. For the relatively weak spectral lines of CS_2, the residuals between them are less than 0.02. In an analogous procedure, the line intensities and self-broadening coefficients of 51 lines from 2179 cm^{-1} to 2182 cm^{-1} are measured and summarized in Table 1. The linear correlation coefficients for line strength and self-broadening summarized in the table are better than 0.995 and 0.99 respectively.

4.3. Air-broadening coefficients measurement

For air-broadening coefficients measurement, the spectrums of mixed CS_2 gas (about 1%) are obtained, divided into several pieces and normalized. By fixing the line strength and Doppler broadening, the spectrums are fitted with Voigt profit to attain the HWHM of collision broadening. The measured and fitted spectrums and the residual between them under eight different pressures near 2181.3 cm^{-1} are presented in Fig. 10. As the contribution of self-collision broadening is only 1% of the whole collision broadening, the different between the self- and

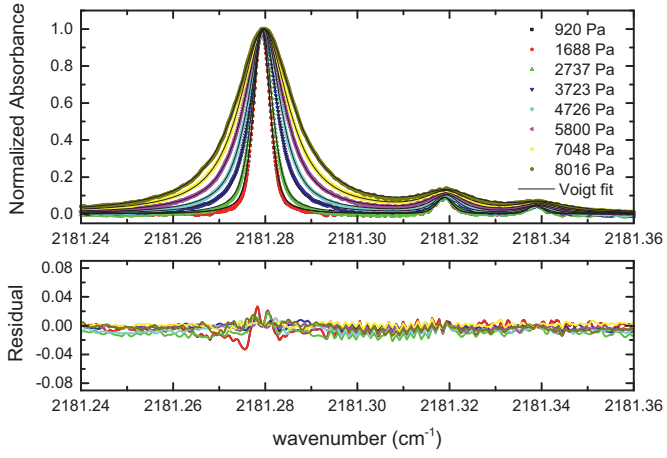

Fig. 10. An example of the recorded absorption spectrum (dots) and the Voigt fitting (line) for the normalized 1% CS_2 mixed sample spectra lines under different pressures (upper panel). Lower panel shows the observed minus calculated residual.

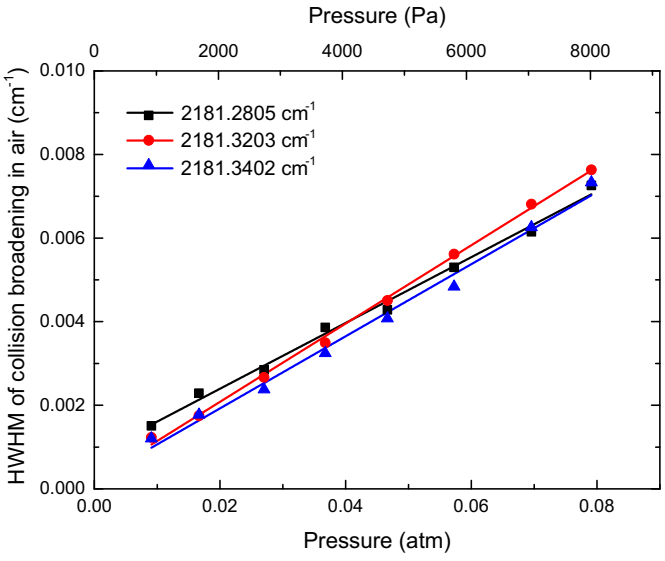

Fig. 11. Example of calculation of air-broadening coefficient for CS_2 spectra lines.

air-broadening coefficients are neglected. The linear correlation coefficients between the gas pressure and the HWHM of collision broadening of the lines in the air are better than 0.99 as demonstrated in Fig. 11. The air-broadening coefficients are 0.0937 cm^{-1}/atm for line at 2181.2805 cm^{-1}, 0.0863 cm^{-1}/atm for line at 2181.3203 cm^{-1} and 0.0821 for line at 2181.3402 cm^{-1}. The linear correlation coefficients of the air-broadening coefficients listed in Table 1 are all better than 0.99.

5. Conclusions

In this work, the positions, intensities, air- and self-broadening coefficients of 51 CS_2 absorption lines between 2179 and 2182 cm^{-1} are carefully investigated based on the quantum cascade laser absorption spectroscopy. The linear correlation coefficients of the fitting results are better than 0.995 for line intensities and 0.99 for air- and self-broadening coefficients. These spectral parameters of the new absorption lines, which are not yet established in HITRAN, would be useful for our developing the calibration-free CS_2 sensor in the near future.

Acknowledgements

This work was supported in part by the National Key Research and Development Program of China (Grant No. 2016YFC0201100 and 2016YFC1400604).

References

[1] S.F. Watts, The mass budgets of carbonyl sulfide, dimethyl sulfide, carbon disulfide and hydrogen sulfide, Atmos. Environ. 34 (2000) 761–779.
[2] S.I. Sulsky, F.H. Hooven, M.T. Burch, K.A. Mundt, Critical review of the epidemiological literature on the potential cardiovascular effects of occupational carbon disulfide exposure, Int. Arch. Occup. Environ. Health 75 (2002) 365–380.
[3] NIOSH, Pocket Guide to Chemical Hazards, NIOSH Publication, 2007.
[4] Emission standards of odor pollutants, GB 14554-93.
[5] M.A. Kamboures, D.R. Blake, D.M. Cooper, R.L. Newcomb, M. Barker, J.K. Larson, S. Meinardi, E. Nussbaum, F.S. Rowland, Breath sulfides and pulmonary function in cystic fibrosis, Proc. Natl. Acad. Sci. U. S. A. 102 (2005) 15762–15767.
[6] Y. Yu, A. Geyer, P. Xie, B. Galle, L. Chen, U. Platt, Observation of carbon disulfide by differential optical absorption spectroscopy in Shanghai, Geophys. Res. Lett. 31 (2014) L11107.
[7] X. Zhang, Z. Cui, Z. Cheng, Y. Li, H. Xiao, Quantitative detection of H_2S and CS_2 mixed gases based on UV absorption spectrometry, RSC Adv. 7 (2017) 50889–50898.
[8] Z. Du, J. Li, X. Cao, H. Gao, Y. Ma, High-sensitive carbon disulfide sensor using wavelength modulation spectroscopy in the mid-infrared fingerprint region, Sensors Actuators B 247 (2017) 384–391.
[9] X. Cao, J. Li, H. Gao, Z. Du, Y. Ma, Simultaneous determination of carbon disulfide, carbon monoxide, and dinitrogen oxide by differential absorption spectroscopy using a distributed feedback quantum cascade laser, Anal. Lett. 50 (2017) 2342–2350.
[10] J.P. Waclawek, H. Moser, B. Lendl, Compact quantum cascade laser based quartz-enhanced photoacoustic spectroscopy sensor system for detection of carbon disulfide, Opt. Express 24 (2016) 6559.
[11] J.P. Waclawek, R. Schmuck, R. Kroismayr, T. Röder, B. Lendl, A new sensor system employing a mid-infrared quantum cascade laser for direct carbon disulfide measurement in an industrial environment, Lenzinger Berichte 92 (2015) 1–5.
[12] S.W. Sharpe, T.J. Johnson, R.L. Sams, P.M. Chu, G.C. Rhoderick, P.A. Johnson, Gas-phase databases for quantitative infrared spectroscopy, Appl. Spectrosc. 58 (2004) 1452–1461.
[13] G. Blanquet, J. Walrand, C. Wèber, M. Lepère, Absolute intensity measurements in the $\nu 3$ band of carbon disulphide, Mol. Phys. 101 (2003) 1911–1917.
[14] M. Lengelé, C. Lerot, G. Blanquet, J. Walrand, J. Bouanich, Pressure broadening study of carbon disulfide for atmospheric detection, Spectrochim. Acta A 59 (2003) 417–420.
[15] P.K. Tshikala, J. Populaire, G. Blanquet, M. Lepère, He-, Ne- and Kr-broadening coefficients of lines in the fundamental $\nu 3$ band of $^{12}C^{32}S_2$ at low temperature, J. Mol. Spectrosc. 298 (2014) 24–30.
[16] P.K. Tshikala, G. Blanquet, M. Lepère, Study of the effect of perturber mass on collisional broadening coefficients of lines in the $\nu 3$ band of CS_2, J. Mol. Spectrosc. 275 (2012) 48–52.
[17] G. Blanquet, J. Walrand, J. Bouanich, Fourier transform spectra of carbon disulfide in the 2800–3000 cm^{-1} region, J. Mol. Struct. 780 (2006) 171–177.
[18] H. Deng, J. Sun, B. Yu, J. Li, Near infrared diode laser absorption spectroscopy of acetylene between 6523 and 6587cm^{-1}, J. Mol. Spectrosc. 314 (2015) 1–5.
[19] I.E. Gordon, L.S. Rothman, C. Hill, R.V. Kochanov, Y. Tan, P.F. Bernath, M. Birk, V. Boudon, A. Campargue, K.V. Chance, B.J. Drouin, J.-M. Flaud, R.R. Gamache, J.T. Hodges, D. Jacquemart, V.I. Perevalov, A. Perrin, K.P. Shine, M.-A.H. Smith, J. Tennyson, G.C. Toon, H. Tran, V.G. Tyuterev, A. Barbe, A.G. Császár, V.M. Devi, T. Furtenbacher, J.J. Harrison, J.-M. Hartmann, A. Jolly, T.J. Johnson, T. Karman, I. Kleiner, A.A. Kyuberis, J. Loos, O.M. Lyulin, S.T. Massie, S.N. Mikhailenko, N. Moazzen-Ahmadi, H.S.P. Müller, O.V. Naumenko, A.V. Nikitin, O.L. Polyansky, M. Rey, M. Rotger, S.W. Sharpe, K. Sung, E. Starikova, S.A. Tashkun, J. Vander Auwera, G. Wagner, J. Wilzewski, P. Wcisło, S. Yu, E.J. Zak, The HITRAN2016 molecular spectroscopic database, J. Quant. Spectrosc. Radiat. Transf. 203 (2017) 3–69.
[20] L.S. Rothman, I.E. Gordon, Y. Babikov, A. Barbe, D.C. Benner, P.F. Bernath, M. Birk, L. Bizzocchi, V. Boudon, L.R. Brown, A. Campargue, K. Chance, L.H. Coudert, V.M. Devi, B.J. Drouin, A. Fayt, J.M. Flaud, R.R. Gamache, J. Harrison, J.M. Hartmann, C. Hill, J.T. Hodges, D. Jacquemart, A. Jolly, J. Lamouroux, R.J. LeRoy, G. Li, D. Long, C.J. Mackie, S.T. Massie, S. Mikhailenko, H.S.P. Müller, O.V. Naumenko, A.V. Nikitin, J. Orphal, V.I. Perevalov, A. Perrin, E.R. Polovtseva, C. Richard, M.A.H. Smith, E. Starikova, K. Sung, S.A. Tashkun, J. Tennyson, G.C. Toon, V.G. Tyuterev, G. Wagner, The HITRAN2012 molecular spectroscopic database, J. Quant. Spectrosc. Radiat. Transf. 130 (2013) 4–50.